The Mechanism of Methoxy Radical Oxidation by O_2 in the Gas Phase. Computational Evidence for Direct H Atom Transfer Assisted by an Intermolecular Noncovalent O···O Bonding Interaction

Josep M. Bofill,[†] Santiago Olivella,*[,†,‡,§] Albert Solé,[⊥] and Josep M. Anglada[‡]

Contribution from the Departaments de Química Orgànica i Química Física, Universitat de Barcelona, Martí i Franquès 1, 08028-Barcelona, Catalunya, Spain, and Departament de Química Orgànica Biològica, CSIC, Jordi Girona 18, 08034-Barcelona, Catalunya, Spain

Received June 2, 1998

Abstract: The mechanism of the $CH_3O^\bullet + O_2$ reaction in the gas phase leading to $CH_2O + HO_2^\bullet$ was studied by using high-level quantum mechanical electronic structure calculations. The CASSCF method with the 6-311G(d,p) basis set was employed for geometry optimization of 15 stationary points on the ground-state potential energy reaction surface and computing their harmonic vibrational frequencies. These stationary points were confirmed by subsequent geometry optimizations and vibrational frequencies calculations by using the CISD and QCISD methods with the 6-31G(d) and 6-311G(d,p) basis sets. Relative energies were calculated at the CCSD(T) level of theory with extended basis sets up to cc-pVTZ at the CASSCF/6-311G(d,p)-optimized geometries. In contrast to a recent theoretical study predicting an addition/elimination mechanism forming the trioxy radical $CH_3OOO^\bullet$ as intermediate, the oxidation of $CH_3O^\bullet$ by O_2 is found to occur by a direct H atom transfer mechanism through a ringlike transition structure of C_s symmetry. This transition structure shows an intermolecular noncovalent O···O bonding interaction, which lowers its potential energy with respect to that of a noncyclic transition structure by about 8 kcal/mol. The 1,4 H atom transfer in $CH_3OOO^\bullet$ is not accompanied by $HO_2^\bullet$ elimination but leads to the trioxomethyl radical $^\bullet CH_2OOOH$ via a puckered ringlike transition structure, lying 50.6 kcal/mol above the energy of the reactants. The direct H atom transfer pathway is predicted to occur with an Arrhenius activation energy of 2.8 kcal/mol and a preexponential factor of 3.5733×10^{-14} molecule cm^3 s^{-1} at 298 K. Inclusion of quantum mechanical tunneling correction to the rate constant computed with these parameters leads to a rate constant of 2.7×10^{-15} $molecule^{-1}$ cm^3 s^{-1} at 298 K, in good agreement with the experimental value of 1.9×10^{-15} $molecule^{-1}$ cm^3 s^{-1}.

I. Introduction

The methoxy radical ($CH_3O^\bullet$) plays a key role in chemical reactions important in both atmospheric and combustion environments.[1] Under atmospheric conditions the $CH_3O^\bullet$ is oxidated by molecular oxygen (O_2, $^3\Sigma_g^-$) forming formaldehyde (CH_2O) and hydroperoxy radical ($HO_2^\bullet$). There are at least three possible pathways for this reaction: (a) by bimolecular hydrogen abstraction through a direct transfer of a H atom from $CH_3O^\bullet$ to O_2

$$CH_3O^\bullet + O_2 \rightarrow CH_2O + HO_2^\bullet \quad (1)$$

(b) by radical addition of $CH_3O^\bullet$ to O_2 forming the methyltrioxy radical $CH_3OOO^\bullet$ (**1**) as intermediate

$$CH_3O^\bullet + O_2 \rightarrow CH_3OOO^\bullet \quad (2)$$

which might undergo an intramolecular 1,4-hydrogen shift, forming the trioxomethyl radical $^\bullet CH_2OOOH$ (**2**)

$$CH_3OOO^\bullet \rightarrow CH_2OOOH^\bullet \quad (3)$$

and subsequent homolytic cleavage of the central OO bond of the latter radical, leading to fragmentation into $CH_2O + HO_2^\bullet$,

$$CH_2OOOH^\bullet \rightarrow CH_2O + HO_2^\bullet \quad (4)$$

and (c) by concerted elimination of $HO_2^\bullet$ from the intermediate radical **1** formed by addition of $CH_3O^\bullet$ to O_2 (eq 2)

$$CH_3OOO^\bullet \rightarrow CH_2O + HO_2^\bullet \quad (5)$$

These reaction pathways are shown in Scheme 1, where **TS1**−**TS5** denote the transition states involved in eqs 1−5, respectively. Which of these routes is responsable for CH_2O formation at low temperatures remains an issue of discussion.

[†] Departament de Química Orgànica, Universitat de Barcelona.
[‡] Departament de Química Orgànica Biològica, CSIC.
[§] E-mail: olivella@taga.qo.ub.es.
[⊥] Departament de Química Física, Universitat de Barcelona.

(1) For a review, see: Atkinson, R. *J. Phys. Chem. Ref. Data Monogr.* **1994**, *2*, 1.
(2) Barker, J. R.; Benson, S. W.; Golden, D. M. *Int. J. Chem. Kinet.* **1977**, *9*, 31.
(3) Batt, L.; Robinson, G. N. *Int. J. Chem. Kinet.* **1979**, *11*, 1045.
(4) Cox, R. A.; Derwent, R. G.; Kearsey, S. V.; Batt, L.; Patrick, K. G. *J. Photochem.* **1980**, *13*, 149.
(5) Niki, H.; Maker, P. D.; Savage, C. M.; Breitenback, L. P. *J. Phys. Chem.* **1981**, *85*, 877.
(6) Gutman, D.; Sanders, N.; Butler, J. E. *J. Phys. Chem.* **1982**, *86*, 66.
(7) Lorenz, K.; Rhasa, D.; Zeller, R.; Fritz, B. *Ber. Bunsen-Ges. Phys. Chem.* **1985**, *89*, 341.
(8) Wantuck, P. J.; Oldenberg, R. C.; Baughcum, S. L.; Winn, K. R. *J. Phys. Chem.* **1987**, *91*, 4653.
(9) *Chemical Kinetics and Photochemical Data for use in Stratospheric Modelong*; Evaluation Number 11, JPL Publication 94-26, 1994.

10.1021/ja981926y CCC: $18.00
Published on Web 01/27/1999

Scheme 1

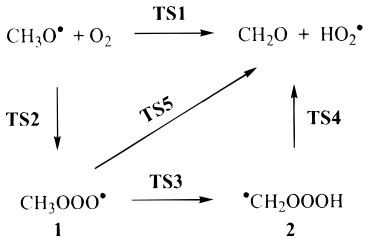

Several investigators[2−8] reported rate constant measurements for reaction eq 1, covering a temperature range of approximately 300−970 K. From these measurements the Jet Propulsion Laboratory Publication 94-26[9] has recommended the parameters $A = 3.9 \times 10^{-14}$ cm^3 molecule^{-1} s^{-1} and $E_a/R = 900 \pm 300$ for the thermal Arrhenius expression of the rate constant for the reaction of $CH_3O^\bullet$ with O_2. Lorenz et al.[7] have observed that the small *A*-factor for this reaction rules out a noncyclic transition state such as that expected for a conventional direct bimolecular H-abstraction reaction eq 1, referred to as **TSA**,

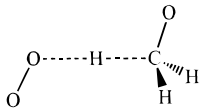

TSA

because the corresponding *A*-factor is expected to be in the range $(3-6) \times 10^{-13}$ cm^3 molecule^{-1} s^{-1}.[10] In discussing their results of the kinetic study for the reaction of isopropoxy radical ($(CH_3)_2CHO^\bullet$) with O_2, Balla et al.[11] have rationalized the small *A*-factors measured for H transfer from alkoxy radicals to O_2 in terms of a tight transition state. As has been noted recently by Wu and Carr[12] in their kinetic study of the reaction of $CFCl_2$-$CH_2O^\bullet$ with O_2, the transition state theory predicts that cyclic transition structures can accommodate *A*-factors even smaller than 10^{-14} cm^3 molecule^{-1} s^{-1}, since the formation of a five-membered ring transition structure from an intermediate trioxy radical $CFCl_2CH_2OOO^\bullet$ requires an entropy change of about -13 cal deg^{-1} mol^{-1} and causes a 3 order of magnitude decrease of the *A*-factor from the normal value. On the other hand, using group additivity rules[13] Hartman et al.[14] have estimated that formation of $CH_3CH_2OOO^\bullet$ from $CH_3CH_2O^\bullet$ and O_2 is sufficiently endoergic to rule out the formation of an intermediate bound complex with a tight transition state. However, a recent ab initio study[15] by Jungkamp and Seinfeld has shown that the group additivity scheme significantly overestimates the enthalpies of formation of trioxy radicals.

To elucidate the mechanism by which $CH_2O + HO_2^\bullet$ is formed and ascertain the nature of the transition state involved, there is a need for rigorous quantum-chemical calculations of the potential energy surface (PES) of the $CH_3O^\bullet + O_2$ reaction. To date the only theoretical study focused on this PES seems to be one recently reported by Jungkamp and Seinfeld.[16] The energetic profiles of pathways (a) and (c) were calculated by using G2M(RCC)[17] and CBS-QCI/APNO[18] model chemistries. The G2M(RCC) calculations were performed at the geometries of stationary points (minima and saddle points) located on the PES using the hybrid density functional theory method known as B3LYP, i.e., Becke's three parameter nonlocal-exchange functional[19] with the nonlocal correlation functional of Lee, Yang, and Parr,[20] employing the d,p-polarized triple split-valence 6-311G(d,p) basis set[21] with Cartesian *d* functions. The CBS-QCI/APNO calculations were carried out at the geometries optimized by using quadratic configuration interaction with the single and double excitations (QCISD) method,[22] based on a reference spin-unrestricted single determinant, employing the 6-311G(d,p) basis set with spherical harmonic *d* functions. The 298 K barrier height for path (a) was found to be 11.5 (14.8) kcal/mol at the G2M(RCC) level (CBS-QCI/APNO value in parentheses). Along path (c), the $HO_2^\bullet$ elimination from the cis isomer of **1** was found to take place via a ringlike transition state with a barrier of 1.3 (8.5) kcal/mol. A schematic drawing of this transition state, referred to as **TSB** (transition structure

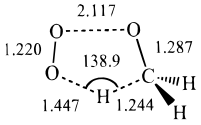

TSB

TS4 in ref 16) is depicted below (distances in Å and angle in deg). Accordingly, Jungkamp and Seinfeld concluded that oxidation of $CH_3O^\bullet$ is likely to occur by an addition/elimination mechanism forming **1** as the intermediate rather than by direct H-abstraction. However, pathway (b), involving the intramolecular 1,4-hydrogen shift **1** → **2**, was not reported in their paper.

At this point it is worth noticing that Schaefer and coworkers[23] have very recently reported a theoretical study on the mechanism of the oxidation of the ethyl radical ($CH_3CH_2^\bullet$) by O_2 forming ethene (CH_2CH_2) and $HO_2^\bullet$. Using the B3LYP method with a triple-ζ plus double-polarization plus f functions (TZ2Pf) basis set they found two distinct but energetically proximate intramolecular hydrogen-transfer transition structures on the ground-state PES of the $CH_3CH_2^\bullet + O_2$ reaction. One of the transition structures corresponds to the transition state for the concerted $HO_2^\bullet$ elimination in the ethylperoxy radical ($CH_3CH_2OO^\bullet$), a reaction analogous to that of eq 5, while the other transition structure corresponds to the transition state for the 1,4-hydrogen shift in $CH_3CH_2OO^\bullet$ leading to the hydroperoxyethyl radical ($^\bullet CH_2CH_2OOH$). Since $CH_3O^\bullet$ and CH_3-$CH_2^\bullet$, as well as CH_2O and CH_2CH_2, are isoelectronic molecules, one would expect similar pathways for the oxidation of $CH_3O^\bullet$ and $CH_3CH_2^\bullet$ by O_2 forming CH_2O and CH_2CH_2, respectively. Accordingly, it is likely that a pathway for the 1,4-hydrogen shift in **1** leading to **2** also exists on the ground-state PES of the $CH_3O^\bullet + O_2$ reaction. To investigate this possibility, we carried out a quantum-chemical investigation of pathway (b). Preliminary B3LYP calculations with the 6-311G(d,p) basis set

(10) Zabarnick, S.; Heicklen, J. *Int. J. Chem. Kinet.* **1985**, *17*, 455.
(11) Balla, R. J.; Nelson, H. H.; McDonald, J. R. *Chem. Phys.* **1985**, *99*, 323.
(12) Wu, F.; Carr, R. W. *J. Phys. Chem.* **1996**, *100*, 9352.
(13) Benson, S. W.; Cruickshank, F. R.; Golden, D. M.; Haugen, G. R.; O'Neal, H. E.; Rodgers, A. S.; Shaw, R.; Waish, R. *Chem. Rew.* **1969**, *69*, 279.
(14) Hartmann, D.; Karthauser, J.; Sawerysyn, J. P.; Zellner, R. *Ber. Bunsen-Ges. Phys. Chem.* **1990**, *94*, 639.
(15) Jungkamp, T. P. W.; Seinfeld, J. H. *Chem. Phys. Lett.* **1996**, *257*, 15.
(16) Jungkamp, T. P. W.; Seinfeld, J. H. *Chem. Phys. Lett.* **1996**, *263*, 371.
(17) Mebel, A. M.; Morokuma, K.; Lin, M. C. *J. Chem. Phys.* **1995**, *103*, 7414.
(18) Montgomery, J. A.; Ochterski, J. W.; Petersson, G. A. *J. Chem. Phys.* **1994**, *101*, 5900.
(19) Becke, A. D. *J. Chem. Phys.* **1993**, *98*, 5648.
(20) Lee, C.; Yang, W.; Parr, R. G. *Phys. Rev. B* **1988**, *37*, 785.
(21) Krishnan, R.; Binkley, J. S.; Pople, J. A. *J. Chem. Phys.* **1980**, *72*, 650.
(22) Pople, J. A.; Head-Gordon, M.; Raghavachari, K. *J. Chem. Phys.* **1987**, *87*, 5968.
(23) Ignatyev, I. S.; Xie, Y.; Allen, W. D. Schaefer, H. F., III *J. Chem. Phys.* **1997**, *107*, 141.

indicated that the intermediate radical **2** is not a stationary point on the PES, while complete active space self-consistent field (CASSCF)[24] calculations with the latter basis predicted **2** to be a local minimum. Furthermore, an intrinsic reaction coordinate (IRC)[25] calculation at the B3LYP/6-31G(d,p) level showed that the ringlike transition structure **TSB** is connected to a hydrogen-bonded [$CH_2O\cdots HOO^\bullet$] complex in the forward direction and to a loosely bound [$CH_3O^\bullet\cdots O_2$] complex, rather than to the intermediate **1**, in the reverse reaction. Therefore, the reaction mechanism conclusions of Jungkamp and Seinfeld were questioned by these results.

In an attempt to clarify how $CH_3O^\bullet$ is oxidated by O_2 in the gas phase, here we present the results of our theoretical investigation. Specifically, we report a complete characterization of 15 stationary points on the ground-state PES of the $CH_3O^\bullet + O_2$ reaction, including predictions of geometrical structures, harmonic vibrational frequencies, absolute entropies, and relative energies of minima and transition structures. Energy differences between the direct H atom transfer and stepwise addition/elimination mechanisms are obtained and rationalized in terms of the structural features shown by the radical intermediates and transition structures involved. Finally, the Arrhenius parameters and rate constant for the rate-determining step of the energetically preferred pathway are compared with the available experimental data.

II. Electronic Structure Considerations

Experimental studies of its electronic and vibrational spectra have established that the electronic ground state of $CH_3O^\bullet$ has C_{3v} molecular symmetry and corresponds to a degenerate ^2E state.[26] The Jahn−Teller theorem predicts that the equilibrium geometry of $CH_3O^\bullet$ will distort to a geometry of lower symmetry wherein the degeneracy will be removed. In fact, previous ab initio electronic structure calculations[27−30] have found a small energy lowering (0.35−0.63 kcal/mol) when the geometry of the electronic ground state ^2E undergoes its Jahn−Teller distortion from C_{3v} to C_s, symmetry leading to a stable nondegenerate ground state $^2A'$. Scheme 2 shows a diagrammatic representation of the electronic structure of the reactants and products for reaction eq 1 assuming that the O_2 molecule abstracts the H atom of $CH_3O^\bullet$ lying in the molecular symmetry plane. Following the convention of Goddard et al.[31] here we have ignored the core orbitals, 1s for carbon, 1s and 2s for oxygen, which are tightly bound and remain relatively unchanged as the atoms are brought together to form the molecules. See Scheme 2 for orbital designations. Dots indicate the number of electrons in each orbital and tie lines indicate the coupling of two singly occupied orbitals into a bonding pair.

At infinite separation the lowest electronic state of the reactants system is a doublet of A″ symmetry, originating from a coupling of the $^2A'$ state of $CH_3O^\bullet$ with the $^3\Sigma_g^-$ state of O_2.

Scheme 2

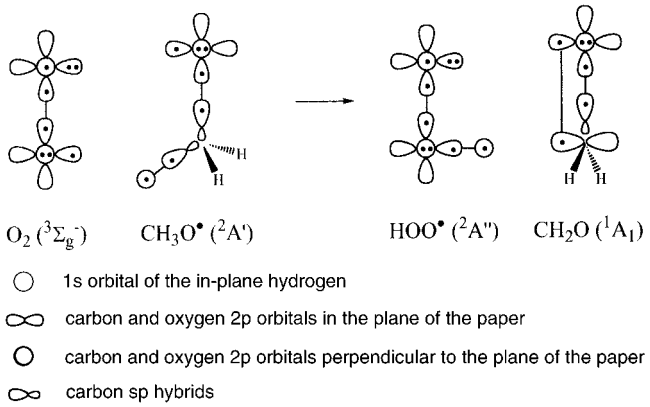

Scheme 3

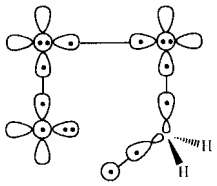

cis-$CH_3OOO^\bullet$ ($^2A''$)

If reaction 1 takes place through direct H-abstraction within C_s symmetry, with the O_2 in-plane, it would initially be assumed the H atom transfer arises simply from the interaction of the 1s orbital of the in-plane H atom of $CH_3O^\bullet$ with the singly occupied in-plane π^* component of O_2. Then it is apparent from Scheme 2 that the ground state of the reactants ($^2A''$) correlates with the $^2A''$ ground state of the products, originating from a coupling of the $^2A''$ state of $HO_2^\bullet$ with the $^1A_1$ state of CH_2O. Therefore, it can be concluded that the direct H-abstraction mechanism of reaction 1 is symmetry-allowed and corresponds to an adiabatic process on the ground-state PES of the $CH_3O^\bullet + O_2$ reaction.

Recent ab initio quantum-chemical calculations[15,16,32] have shown that the methyltrioxy radical **1** exhibits two distinct minima on the $^2A''$ electronic ground-state PES corresponding to the cis and trans conformal stereoisomers of C_s symmetry. The G2M(RCC) and CBS-APNO formalisms predict the trans isomer to be 1.14 and 0.97 kcal/mol, respectively, higher in energy than the cis isomer. Scheme 3 depicts a diagrammatic representation of the electronic structure of *cis*-**1** with the in-plane H atom directed toward the terminal O atom. As seen in Scheme 3, the unpaired electron of *cis*-**1** is localized on an out-of-plane 2p orbital of the terminal O atom. This key feature strongly suggests that the 1,4-hydrogen shift **1** → **2** should take place via a puckered (C_1 symmetry) ringlike transition structure to allow the interaction between the 1s orbital of a H atom of the CH_3 group and the singly occupied 2p orbital of the terminal O atom. However, if one assumes that prior to the 1,4-hydrogen shift in *cis*-**1** the central OO bond is stretched until the two electrons forming this bond become uncoupled, the electronic structure of *cis*-**1** may be depicted as a combination of the two valence bond structures shown in Scheme 4. In this situation the 1s orbital of the in-plane H atom can interact with the singly occupied in-plane 2p orbital of the terminal O atom forming a planar (C_s symmetry) ringlike transition structure such as **TSB** leading to CH_2O plus $HO_2^\bullet$. However, when the central OO bond in *cis*-**1** is partially broken, the direct dissociation of *cis*-**1** into $CH_3O^\bullet + O_2$, rather than the H-transfer process, would also be possible.

(24) For a review, see: Roos, B. O. *Adv. Chem. Phys.* **1987**, *69*, 399.
(25) (a) Fukui, K. *Acc. Chem. Res.* **1981**, *14*, 363. (b) Ishida, K.; Morokuma, K.; Kormornicki, A. *J. Chem. Phys.* **1977**, *66*, 2153. (c) Schmidt, M. W.; Gordon, M. S.; Dupuis, M. *J. Am. Chem. Soc.* **1985**, *107*, 7, 2585.
(26) Liu, X.; Damo, C. P.; Lin, T.-Y. D.; Foster, S. C.; Misra, P.; Yu, L.; Miller, T. A. *J. Phys. Chem.* **1989**, *93*, 2266.
(27) Yarkony, D. R.; Schafer, H. F., III; Rothenberg, S. *J. Am. Chem. Soc.* **1974**, *96*, 656.
(28) Bent, G. D.; Adams G. F., Bartram, R. H.; Purvis, G. D.; Bartlett, R. J. *J. Chem. Phys.* **1982**, *76*, 4144.
(29) Saebo, S.; Radom, L.; Schaefer, H. F., III *J. Chem. Phys.* **1983**, *78*, 845.
(30) Page, M.; Lin, M. C.; He, Y.; Choudhury, T. K. *J. Phys. Chem.* **1989**, *93*, 4404.
(31) Goddard, W. A., III; Dunning, T. H.; Hunt, W. J.; Hay, P. J. *Acc. Chem. Res.* **1973**, *6*, 368.
(32) Vicent, A.; Hillier, I. H. *J. Phys. Chem.* **1995**, *99*, 3109.

Scheme 4

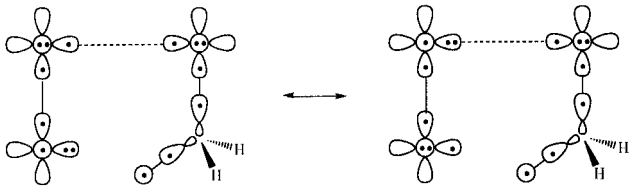

III. Methods and Computational Details

The geometries of the relevant stationary points on the $[CH_3O_3]^\bullet$ ground-state PES were initially optimized by using the spin-unrestricted Hartree−Fock (UHF) version of the self-consistent field (SCF) molecular orbital (MO) method[33] with the d-polarized split-valence 6-31G(d) basis set[34] employing analytical gradient procedures.[35,36] All these ab initio calculations were performed with the GAUSSIAN 94 program package.[37]

The UHF wave function of several calculated transition structures (i.e., **TS1**−**TS4**) was subjected to very serious spin contamination, S^2 ranging from 0.814 to 1.564 as compared to 0.75 for a pure doublet state. This can be taken as an indication of strong nondynamical electron correlation effects. One may then question the reliability of the geometries calculated at the UHF level of theory for these structures. Accordingly, all the geometries (minima and saddle points) were reoptimized by use of multiconfiguration SCF (MCSCF) wave functions of the CASSCF class[24] with the 6-311G(d,p) basis set employing analytical gradient procedures.[36,38] The complete active spaces were selected following the procedure recently suggested by Anglada and Bofill,[39] based on the fractional occupation of the natural orbitals generated from the first-order density matrix calculated from an initial multireference single- and double-excitation configuration interaction (MRDCI) wave function correlating all valence electrons. All CASSCF geometry optimizations were carried out by using the GAMESS system of programs.[40]

All the stationary points were characterized by their harmonic vibrational frequencies as minima or saddle points. The harmonic vibrational frequencies were obtained by diagonalizing the mass-weighted Cartesian force constant matrix calculated analytically at the CASSCF/6-311G(d,p) level by using GAUSSIAN 94. Connections of the transition structures between designated minima were confirmed in each case by IRC calculations[25] at the latter level of theory by using the second-order algorithm of Gonzalez and Schlegel[41] implemented into GAMESS, with a step size of 0.15 bohr·amu$^{1/2}$.

To asses the reliability of the CASSCF results, the geometries and harmonic vibrational frequencies of the most relevant stationary points were also calculated by using the configuration interaction with all single and double excitations (CISD)[42] and quadratic CISD (QCISD)[22] methods, based on a reference UHF single determinant, with core electrons excluded from correlation treatment (frozen core approximation), employing the 6-31G(d) and 6-311G(d,p) basis sets.

To incorporate the effect of dynamical valence-electron correlation on the relative energy ordering of the stationary points located at the CASSCF/6-311G(d,p) level, we carried out single-point (frozen core) coupled-cluster[43] calculations including all single and double excitations, based on a reference UHF single determinant, together with a perturbative treatment of all connected triple excitations[44] (CCSD(T)). To establish that our results were converged with respect to the basis set, the CCSD(T) calculations were carried out with the 6-311G(d,p), 6-311+G(d,p)[45] (which includes a single additional difusse sp shell on heavy atoms only), 6-311+G(3df,2p)[45] (which includes triple d-polarization and a single additional f-polarization on heavy atoms and double p-polarization on hydrogen atoms), and Dunning's correlation-consistent polarized valence triple-ζ (cc-pVTZ) basis sets.[46] Finally, total energies for relevant stationary points were also evaluated from partially spin-adapted CCSD(T) calculations based on a restricted open-shell Hartree−Fock reference determinant (RCCSD(T)[47]) to accomplish the spin contamination problem in spin-unrestricted coupled-cluster wave functions.[48] The cc-pVTZ basis set was used in the latter calculations. The CISD, QCISD, and CCSD(T) calculations were carried out with the GAUSSIAN 94 program, whereas the MOLPRO 96[49] program package was employed for the RCCSD(T) calculations.

Zero-point vibrational energies (ZPVEs) were determined from harmonic vibrational frequencies calculated at the CASSCF/6-311G(d,p) level. Our best total energies at 0 K correspond to the sum of the RCCSD(T)/cc-pVTZ energy and ZPVE correction. Thermal energy (TE) corrections and absolute entropies (S) were obtained, assuming ideal gas behavior, from the harmonic frequencies and moments of inertia by standard methods.[50] A standard pressure of 1 atm was taken in the S calculations. The TE correction to the RCCSD(T)/cc-pVTZ + ZPVE energy was evaluated as a sum of the translational and rotational energies at the absolute temperature T and the change in the vibrational energy in going from 0 to T K. The activation energy (E_a) and preexponential factor (A) of the thermal Arrhenius expression of the second-order rate constant for reaction eq 1 were calculated by the following relations:

$$E_a = \Delta E^{\ddagger} + RT \tag{6}$$

$$A = (e^2 kT/h) \exp(\Delta S_c^{\ddagger}/R) \tag{7}$$

where $\Delta E^{\ddagger}$ and $\Delta S_c^{\ddagger}$ are the energy and entropy (for standard states expressed in concentration units) changes between the reactants and the transition structure of the rate-determining step, R is the ideal gas constant, k is the Boltzmann constant, and h is the Plank constant. $\Delta E^{\ddagger}$ was calculated as follows:

$$\Delta E^{\ddagger} = V^{\ddagger} + \Delta\mathrm{ZPVE} + \Delta E(T) \tag{8}$$

where $V^{\ddagger}$ is the potential energy barrier (calculated at the RCCSD(T)/cc-pVTZ level) and ΔZPVE and $\Delta E(T)$ are the differences between the transition state and reactant ZPVE and TE corrections, respectively. $\Delta S_c^{\ddagger}$ was calculated by the following relation:

(33) Pople, J. A.; Nesbet, R. K. *J. Chem. Phys.* **1954**, *22*, 571.
(34) (a) Hehre, W. J.; Ditchfield, R.; Pople, J. A. *J. Chem. Phys.* **1972**, *56*, 2257. (b) Hariharan, P. C.; Pople, J. A. *Theor. Chim. Acta*. **1973**, *28*, 213
(35) Schlegel, H. B. *J. Comput. Chem*. **1982**, *3*, 214.
(36) Bofill, J. M. *J. Comput. Chem.* **1994**, *15*, 1.
(37) Frisch, M. J.; Trucks, G. W.; Schlegel, H. B.; Gill, P. M. W.; Johnson, B. G.; Robb, M. A.; Cheeseman, J. R.; Keitth, T. A.; Petersson, G. A.; Montgomery, J. A.; Raghavachari, K.; Al-Laham, M. A.; Zakrzewski, V. G.; Ortiz, J. V.; Foresman, J. B.; Cioslowski, J.; Stefanov, A.; Nanayakkara, A.; Challacombe, M.; Peng, C. Y.; Ayala, P. Y.; Chen, W.; Wong, M. W.; Andres, J. L.; Replogle, E. S.; Gomperts, R.; Martin, R. L.; Fox, D. J.; Binkley, J. S.; Defrees, D. J.; Baker, J.; Stewart, J. J. P.; Head-Gordon, M.; Gonzalez, C.; Pople, J. A. *GAUSSIAN 94*; Gaussian, Inc.: Pittsburgh, PA, 1995.
(38) (a) Baker, J. *J. Comput. Chem.* **1986**, *7*, 385. (b) Baker, J. *J. Comput. Chem.* **1987**, *8*, 563.
(39) Anglada, J. M.; Bofill, J. M. *Theor. Chim. Acta* **1995**, *92*, 369.
(40) Schmidt, M. W.; Baldrige, K. K.; Boatz, J. A.; Elbert, S. T.; Gordon, M. S.; Jensen; J.; Koseki, S.; Matsunaga, N.; Nguyen, K. A.; Su, S.; Windus, T. L.; Dupuis, M.; Montgomery, J. A. *J. Comput. Chem.* **1993**, *14*, 1347.
(41) (a) Gonzalez, C.; Schlegel, B. *J. Chem. Phys.* **1989**, *90*, 2154. (b) Gonzalez, C.; Schlegel, B. *J. Phys. Chem.* **1990**, *94*, 5523.
(42) Pople, J. A.; Seeger, R.; Krishnan, R. *Int. J. Quantum Chem. Symp.* **1977**, *11*, 149.
(43) For a review, see: Bartlett, R. J. *J. Phys. Chem.* **1989**, *93*, 1967.
(44) Raghavachari, K.; Trucks, G. W.; Pople. J. A.; Head-Gordon, M. *Chem. Phys. Lett.* **1989**, *157*, 479.
(45) Frisch, M. J.; Pople, J. A.; Binkley. J. S. *J. Chem. Phys.* **1984**, *80*, 3265.
(46) Dunning, T. H. *J. Chem. Phys.* **1989**, *90*, 1007.
(47) Knowles, P. J.; Hampel, C.; Werner, H.-J. *J. Chem. Phys.* **1993**, *99*, 5219.
(48) (a) Purvis, G. D.; Bartlett, R. J. *J. Chem. Phys.* **1982**, *76*, 1910. (b) Hampel, C.; Peterson, K. A.; Werner, H.-J. *Chem. Phys. Lett.* **1992**, *190*, 1. (c) Deegan, M. J. O.; Knowles, P. J. *Chem. Phys. Lett.* **1994**, *227*, 321.
(49) MOLPRO 96: Werner, H.-J.; Knowles, P. J. with contributions from Almlöf, J.; Amos, R. D.; Berning, A.; Deegan, M. J. O.; Eckert, S. T.; Elbert, S. T.; Hampel, C.; Lindh, R.; Meyer, W.; Nicklass, A.; Peterson, K.; Pitzer, R.; Stone, A. J.; Taylor, P. R.; Mura, M. E.; Pulay, P.; Schuetz, M.; Stoll, H.; Thorsteinsson, T.; Cooper, D. L.
(50) See, e.g.: McQuarrie, D. *Statistical Mechanics;* Harper and Row: New York, 1986.

$$\Delta S_c^{\ddagger} = \Delta S^{\ddagger} + R \ln(R'T) \quad (9)$$

where $\Delta S^{\ddagger}$ is the entropy change for standard states expressed in pressure units and R' the ideal gas constant in liter atmosphere units, that is, 0.082 L atm/(mol·K).

Tunneling correction to the rate constant was calculated by zero-order approximation to the vibrationally adiabatic PES model with zero curvature.[51] In this approximation the tunneling is assumed to occur along a unidimensional minimum energy path. The potential energy curve is approximated by an unsymmetrical Eckart potential energy barrier[52] that is required to go through the ZPVE corrected energies of the reactants, transition state, and products. The equations that describe the Eckart potential energy function were adapted from Truong and Truhlar.[51] Solving the Schroedinger equation for the Eckart function yields the transmission probability, $\kappa(E)$. The tunneling correction, $\Gamma^*(T)$, is obtained as the ratio between the quantum mechanical and the classical rate constants calculated by integrating the respective $\kappa(E)$, over all possible energies:

$$\Gamma^*(T) = \frac{\exp((\Delta V^{\ddagger} + \Delta \mathrm{ZPVE})/kT)}{kT} \int_0^{\infty} \exp\left(-\frac{E}{kT}\right) \kappa(E)\, dE \quad (10)$$

To examine the characteristics of the bonding and interactions in the most relevant structures we have also performed an analysis of the electronic charge density within the framework of the topological theory of atom in molecules (AIM) making use of the PROAIM and EXTREME programs of Bader et al.[53] and the MORPHY 97 programs.[54] The first-order electron density matrix obtained from the CASSCF/6-311G(d,p) wave function and the **Z** density matrix determined from QCISD/6-311G(d,p) gradient calculations[55] were used in this analysis. The theory of AIM has been reviewed in a monograph[56] and in a recent review.[57]

IV. Results and Discussion

Selected geometrical parameters of the CASSCF/6-311G(d,p)-optimized structures of all reactants, products, intermediates, and transition states are shown in Figures 1−5. For the purpose of comparison, the geometrical parameters of the structures optimized at the QCISD/6-311G(d,p) level are given in parentheses.[58] Some of these QCISD/6-311G(d,p)-optimized structures (i.e.; **TS1**, **TS1′**, **TS2**, **TSGT**, *trans*-**1**, and *cis*-**1**) have been reported previously.[16] Relative energies calculated at the CCSD(T) level of theory with different basis sets are given in Table 1. In addition, Table 1 includes the ZPVEs, as well as the TE corrections and absolute entropies calculated at 298 K. Tables S1−S3 (Supporting Information) contain the total energies calculated at various levels of theory with different basis sets. Figure 6 summarizes the potential energy profiles calculated at the CCSD(T)/cc-pVTZ level for pathways (a) and (b). These profiles only include the most relevant stationary points located on the PES. Calculated topological properties of the bond critical points and net atomic charges in **TS1** and **TS1′**, determined from Bader AIM analysis of the CASSCF/6-311G-(d,p) and QCISD/6-311G(d,p) electron charge densities, are given in Table 2 and Table S4 (Supporting Information), respectively. Finally, the net atomic charges of the most relevant structures calculated from Bader Population Analysis at the CASSCF/6-311G(d,p) and QCISD/6-311G(d,p) levels are available as Supporting Information (Tables S5 and S6).

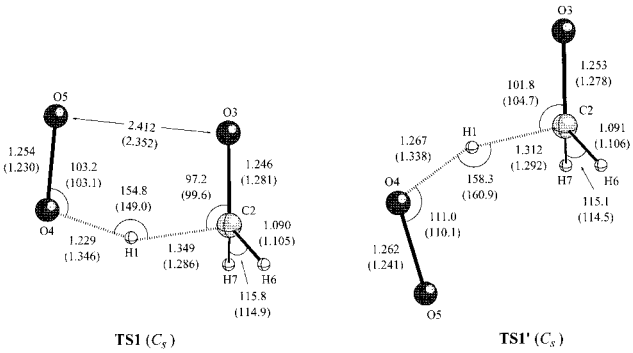

Figure 1. Selected parameters of the CASSCF/6-311G(d,p) optimized geometries of the transition structures (**TS1** and **TS1′**) for direct H atom transfer from $CH_3O^{\bullet}$ to O_2. The QCISD/6-311G(d,p) optimized geometrical parameters are given in parentheses. Distances are given in angstroms and angles in degrees.

A. Direct H Atom Transfer Mechanism. Reaction 1 is predicted to be exoergic by 26.5 kcal/mol at the RCCSD(T)/cc-pVTZ level of computation. Inclusion of the ZPVE and TE corrections leads to an energy of reaction of −26.6 and −26.3 kcal/mol at 0 and 298 K, respectively. The latter value is in excellent agreement with the ΔH_r of −26.2 kcal/mol at 298 K obtained from experimental ΔH_f.[59]

We have found two transition structures, **TS1** and **TS1′** (Figure 1), for direct H atom transfer from $CH_3O^{\bullet}$ to O_2. Both have C_s symmetry and correspond to the lowest $^2A''$ electronic state. **TS1** and **TS1′** differentiates one from the other in the following conformations: **TS1**, with the OO bond in the *cis* position toward the CO bond, and **TS1′**, with the OO bond in the *trans* position. In both transition structures the C2H1O4 angle deviates significantly from the expected value of 180° for a typical H atom transfer from a C atom to an O atom. Although the geometrical parameters computed at the CASSCF and QCISD levels of theory for **TS1** and **TS1′** are qualitatively in agreement, it is apparent (see Figure 1) that the CASSCF transition structures are somewhat closer to the products than in the case of the QCISD transition structures. Thus in the transition structures computed at the CASSCF level the moving H1 atom is located closer to the O4 than to the C2 atom, the C═O double bond is nearly formed, and the radical center is shifted to the out-of-plane p-orbital of the O5 atom of the dioxygen moiety. On the basis that the UHF wave functions underlying the QCISD calculations of **TS1** and **TS1′** show a high spin contamination, as indicated by the S^2 values of 1.6334 (**TS1**) and 1.6755 (**TS1′**), we adopt the reasonable view that the CASSCF optimized structures are more reliable.

The IRC calculations at the CASSCF level of theory showed that both **TS1** and **TS1′** go backward to a loosely bound [$CH_3O^{\bullet}$···O_2] complex. The optimized geometry of this complex, **CX1** (Figure 2), was characterized as a true local minimum on the PES. At the CCSD(T)/cc-pVTZ level, **CX1** lies only 0.6 kcal/

(51) Truong, T. N.; Truhlar, D. G. *J. Chem. Phys.* **1990**, *93*, 1761.
(52) Eckart, C. *Phys. Rev.* **1930**, *35*, 1303.
(53) (a) Biegler-König, F. W.; Bader, R. F. W.; Tang, T.-H. *J. Comput. Chem.* **1982**, *3*, 317. (b) Bader, R. F. W.; Tang, T.-H.; Tal, Y.; Biegler-König, F. W. *J. Am. Chem. Soc.* **1982**, *104*, 946.
(54) (a) MORPHY 97: Popelier, P. L. A. with contributions from Bone, R. G. A.; UMIST: Manchester, UK. 1997. (b) Popelier, P. L. A. *Comput. Phys. Commun.* **1998**, *108*, 180.
(55) See, e.g.: Wiberg, K. B.; Hadad, C. M.; LePage, T.; Breneman, C. M.; Frisch, M. J. *J. Phys. Chem.* **1992**, *96*, 671.
(56) Bader, R. F. W. *Atoms in Molecules: A Quantum Theory*; Clarendon: Oxford, 1990.
(57) Bader, R. F. W.; Popelier, P. L. A.; Keith, T. A. *Angew. Chem., Int. Ed. Engl.* **1994**, *33*, 620.
(58) A full set of Cartesian coordinates for all stationary points as obtained by the different methods see available upon request from the corresponding author.
(59) $\Delta H_f(CH_3O^{\bullet}) = 4.0 \pm 1.0$ kcal/mol,[60] $\Delta H_f(HO_2^{\bullet}) = 3.8 \pm 1.2$ kcal/mol,[61] and $\Delta H_f(CH_2O) = -26.0 \pm 0.2$ kcal/mol at 298 K. For the latter value see ref 62.
(60) Ruscic, B.; Berkowitz, J. *J. Chem. Phys.* **1991**, *95*, 4033.
(61) Fisher, E. R.; Armentrout, P. B. *J. Phys. Chem.* **1990**, *94*, 4396.
(62) Lias, S. G.; Bartmess, J. E.; Liebman, J. B.; Holmes, J. L.; Levin, R. D.; Mallard, W. G. *J. Phys. Chem. Ref. Data* **1988**, *17*, 168.

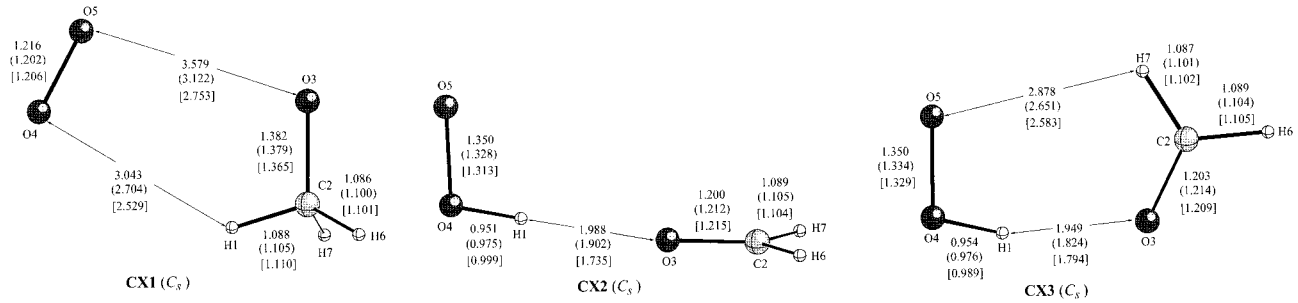

Figure 2. Selected parameters of the CASSCF/6-311G(d,p) optimized geometries of the loosely bound [$CH_3O^{\bullet}\cdots O_2$] complex (**CX1**) and the hydrogen-bonded [$H_2CO\cdots HOO^{\bullet}$] complexes (**CX2**, **CX3**). The QCISD/6-311G(d,p) and B3LYP/6-311G(d,p) optimized geometrical parameters are given in parentheses and square brackets, respectively. Distances are given in angstroms and angles in degrees.

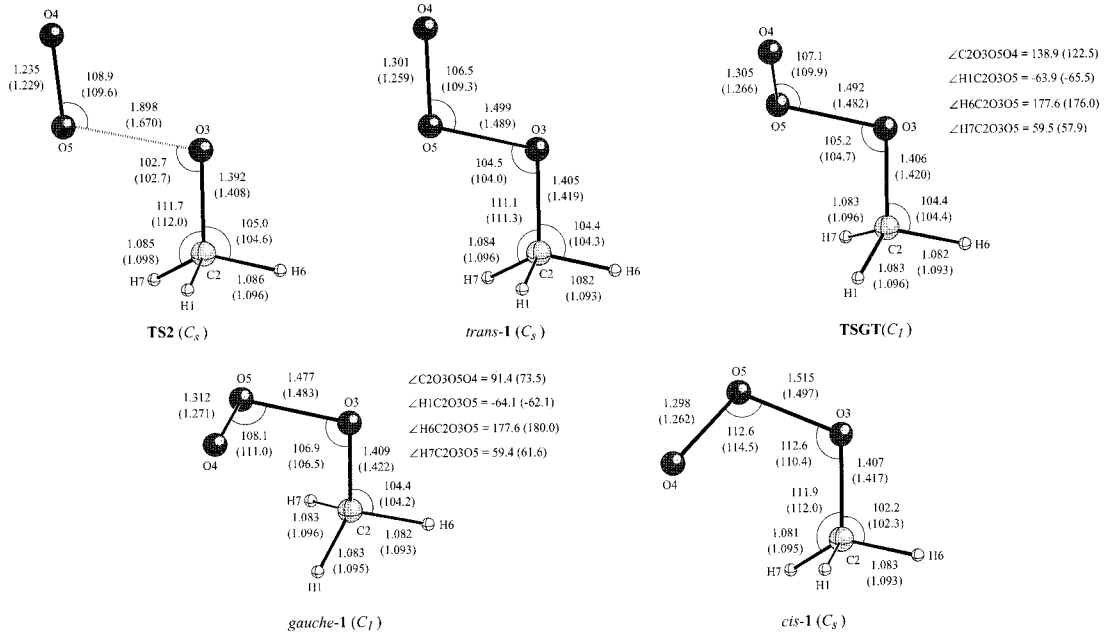

Figure 3. Selected parameters of the CASSCF/6-311G(d,p) optimized geometries of the transition structure (**TS2**) for the addition of $CH_3O^{\bullet}$ to O_2, the trans (*trans*-**1**), gauche (*gauche*-**1**), and cis (*cis*-**1**) conformers of the intermediate $CH_3OOO^{\bullet}$, and the transition structure (**TSGT**) connecting *trans*-**1** and *gauche*-**1**. The caption for Figure 1 describes the assumed notation.

mol below the energy of the isolated reactants. Inclusion of the correction for the basis set superposition effects (BSSE), calculated by using the counterpoise method,[63,64] leads to a stabilization energy of **CX1** toward decomposition into $CH_3O^{\bullet}$ + O_2 of 0.3 kcal/mol at the CCSD(T)/cc-pVTZ level of computation. The above IRC calculations for the forward direction established that both **TS1** and **TS1′** lead to a hydrogen-bonded [$H_2CO\cdots HOO^{\bullet}$] complex. The optimized geometry of this complex, **CX2** (Figure 2), has one imaginary harmonic vibrational frequency corresponding to the rotation of the methylene group around the C2O3 bond. A geometry reoptimization of **CX2**, slightly modified according to the this normal mode, led to a local minimum, **CX3** (Figure 2), which appears to be a [$H_2CO\cdots HOO^{\bullet}$] complex showing a short (1.949 Å) and a long (2.878 Å) hydrogen bond. At the CCSD(T)/cc-pVTZ level of computation, this complex lies 9.0 kcal/mol below the energy of the isolated products. The correction for BSSE leads to a stabilization energy of **CX3** toward decomposition into CH_2O + $HO_2^{\bullet}$ of 8.1 kcal/mol. Inclusion of the ZPVE correction to the latter value gives a stabilization energy of 6.1 kcal/mol at 0 K.

At this point it is important to note that the geometry optimized at the QCISD/6-311G(d,p) level of computation for **TS1** (Figure 1) and its total energy (Table S3, Supporting Information) are identical with those found by Jungkamp and Seinfeld at the same level for **TSB**, namely the transition structure that should connect the intermediate *cis*-**1** and the products CH_2O + $HO_2^{\bullet}$. However, IRC calculations at the QCISD level with both the 6-31G(d) and 6-31G(d,p) basis sets, starting at the corresponding optimized structure of **TS1**, confirmed in each case that **TS1** connects the complexes **CX1** and **CX2**, rather than *cis*-**1** and CH_2O + $HO_2^{\bullet}$. This important discrepancy will be discussed later.

At the CASSCF/6-311G(d,p) level **TS1** is calculated to be 3.7 kcal/mol less energetic than **TS1′** (see Table S1). On the basis that the O5O3 distance in **TS1** (2.412 Å) is 0.388 Å shorter than twice the oxygen atom van der Waals nonbonded radius (1.40 Å),[65] one would expect **TS1** to be higher in energy than **TS1′** owing to the electrostatic repulsion between the lone pairs on the O5 and O3 atoms in **TS1**. Furthermore, the absolute entropy of **TS1** at 298 K is calculated to be 7.6 eu lower than the entropy of **TS1′**, so the former transition structure is "tighter" than the latter. How can the energy difference between **TS1** and **TS1′** be rationalized? We begin by comparing the results of the topological analysis of the electronic charge density in **TS1** and **TS1′**. Figure 7 displays the contour plot of the electronic charge density for **TS1** in the C_s symmetry plane.

(63) Boys, S. F.; Bernardi, F. *Mol. Phys.* **1970**, *19*, 553.

(64) van Duijneveldt, F. B.; van Duijneveldt-van de Rijdt, J. G. C. M.; van Lenthe, J. H. *Chem. Rev.* **1994**, *94*, 1873.

(65) Pauling, L. C. *The Nature of the Chemical Bond;* Cornell University Press: Ithaca, NY, 1960.

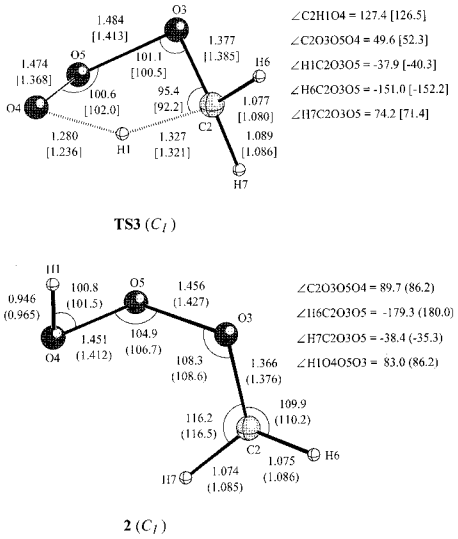

Figure 4. Selected parameters of the CASSCF/6-311G(d,p) optimized geometries of the transition structure (**TS3**) for the 1,4-hydrogen shift in $CH_3OOO^{\bullet}$ and the intermediate $^{\bullet}CH_2OOOH$ (**2**). The CISD/6-311G-(d,p) optimized geometrical parameters of **TS2** are given in square brackets and the QCISD/6-311G(d,p) optimized geometrical parameters of **2** are given in parentheses. Distances are given in angstroms and angles in degrees.

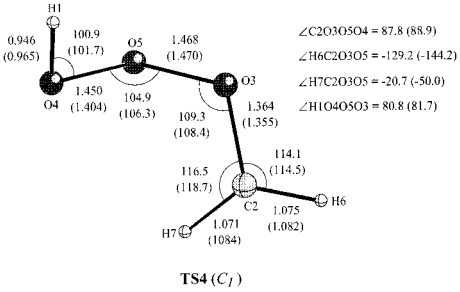

Figure 5. Selected parameters of the CASSCF/6-311G(d,p) optimized geometries of the transition structure (**TS4**) for the fragmentation of $^{\bullet}CH_2OOOH$ into $CH_2O + HO_2^{\bullet}$. The caption for Figure 1 describes the assumed notation.

The crucial feature is that in **TS1** exists an extra bond critical point located between the oxygen atoms O5 and O3. As shown by the data in Table 2, this bond critical point is somewhat closer to O3 than to O5. We recall that a bond critical point between two atoms indicates the presence of a binding interaction between these atoms. Consequently, the lower energy of **TS1** with respect to **TS1′** can be ascribed to a binding interaction between the terminal oxygen atoms in **TS1**, which is lacking in **TS1′** due to the long distance between these atoms.

The origin of the unexpected binding interaction between the terminal oxygen atoms in **TS1** can be elucidated by analyzing the topological properties of the bond critical point found between these atoms (see Table 2). Thus the relatively low value of the electronic charge density ($\rho_b = 0.0262$ au) and the positive value of its Laplacian ($\nabla^2\rho_b = 0.1030$ au) at this bond critical point indicate that O5 and O3 are bound by a closed-shell interaction. According to the net atomic charges calculated for atoms O3 and O5 (i.e., -0.972 and -0.016 *e*, respectively), there is a large accumulation of negative charge within the basin of the O3 atom, while the negative charge within the basin of the O5 atoms is remarkably small. Since the net atomic charge on the oxygen atom in $CH_3O^{\bullet}$ is calculated to be -0.678 *e* (see Table S5), the large negative net charge on the O3 atom in **TS1** arises from the transfer of charge from C2 to O3 due to the formation of a π bond between these atoms. In fact, the ellipticity of the C2O3 bond in **TS1** ($\epsilon = 0.1179$) is nearly identical to that calculated (0.1161) for the C=O double bond in CH_2O. Figure 8 shows the contour plot in the C_s symmetry plane of the MO associated to the forming π bond between the C2 and O3 atoms in **TS1**. It is worth noting that one side of this π orbital is directed toward the O5 atom. Due to the large accumulation of negative charge within the basin of the O3 atom, the nucleus of the O5 atom is attracted by the large net negative field exerted on it by the O3 atom, and the electronic charge distribution in the basin of the O5 atom must polarize away from the O3 atom to balance this net attractive force on its nucleus. On the other hand, the nucleus of the O5 atom attracts the electronic charge distribution in the basin of the O3 atom so it must polarize toward the O5 atom. Thus, the terminal oxygen atoms in **TS1** are bound due to the polarization of both atoms caused by the forces exerted on their nuclei by the electronic charge accumulated on the O3 atom, which arises chiefly from the forming C2O3 π bond.

The energy difference of 3.7 kcal/mol between **TS1′** and **TS1**, predicted by the CASSCF/6-311G(d,p) calculations, rises to 7.5 kcal/mol at the CCSD(T)/6-311G(d,p) level. This result indicates that the dynamical valence-electron correlation lowers the energy of **TS1** with respect to **TS1′**. On the other hand, Table 1 shows that the basis set extension does not change significantly the relative energy of these transition structures. Therefore, it can be concluded that the preferred route for direct H atom transfer from $CH_3O^{\bullet}$ to O_2 takes place through **TS1**. Further support to this transition structure is provided by the predicted activation entropy of -35.3 cal mol^{-1} K^{-1}, calculated at 298 K from the absolute entropies for the reactants and **TS1**. This value is in excellent agreement with the value of -35.1 cal mol^{-1} K^{-1} determined from the recommended[9] experimental Arrhenius preexponential factor $A = 3.9 \times 10^{-14}$ cm^3 molecule^{-1} s.$^{-1}$

B. Stepwise Mechanism. The first step of pathway (b) consists of the formation of the trans isomer of the methyltrioxide radical, *trans*-**1** (Figure 3), via a transition structure of C_s symmetry, **TS2** (Figure 3), when the oxygen molecule attaches to the radical site of $CH_3O^{\bullet}$. This process is predicted to be endoergic by 4.8 kcal/mol with a potential energy barrier of 7.4 kcal/mol. At the RCCSD/cc-pVTZ level of computation this barrier is lowered to 5.6 kcal/mol. Thus the potential energy barrier for the formation of *trans*-**1** is only 1.8 kcal/mol higher than the barrier calculated at the same level for the direct H atom transfer from $CH_3O^{\bullet}$ to O_2 via **TS1**. Inclusion of the ZPVE corrections increases to 4.5 kcal/mol the energy barrier difference between these two competing reactions.

In addition to the trans conformer of the radical intermediate **1**, the CASSCF/6-311G(d,p) calculations predict the existence of a gauche minimum of this radical, *gauche*-**1** (Figure 3), lying only 0.2 kcal/mol below *trans*-**1**. This prediction is in good agreement with the results of both CISD and QCISD calculations with the 6-31G(d) and 6-311G(d,p) basis set, which also predict the gauche conformer of **1** to be a local minimum. In contrast, no stationary point on the PES was found for the gauche isomer of **1** at the B3LYP/6-311G(d,p) level of computation. A torsional transition structure, **TSGT** (Figure 3), connecting the *gauche*-**1** and *trans*-**1** local minima was located at the CASSCF, CISD, and QCISD levels of theory with the 6-31G(d) and 6-311G-(d,p) basis sets. It is worth noting that **TSGT** corresponds to the transition structure **TS3** of Jungkamp and Seinfeld's paper,[16] located at the B3LYP/6-311G(d,p) and QCISD/6-311G(d,p) levels of computation, which was erroneously assigned to the

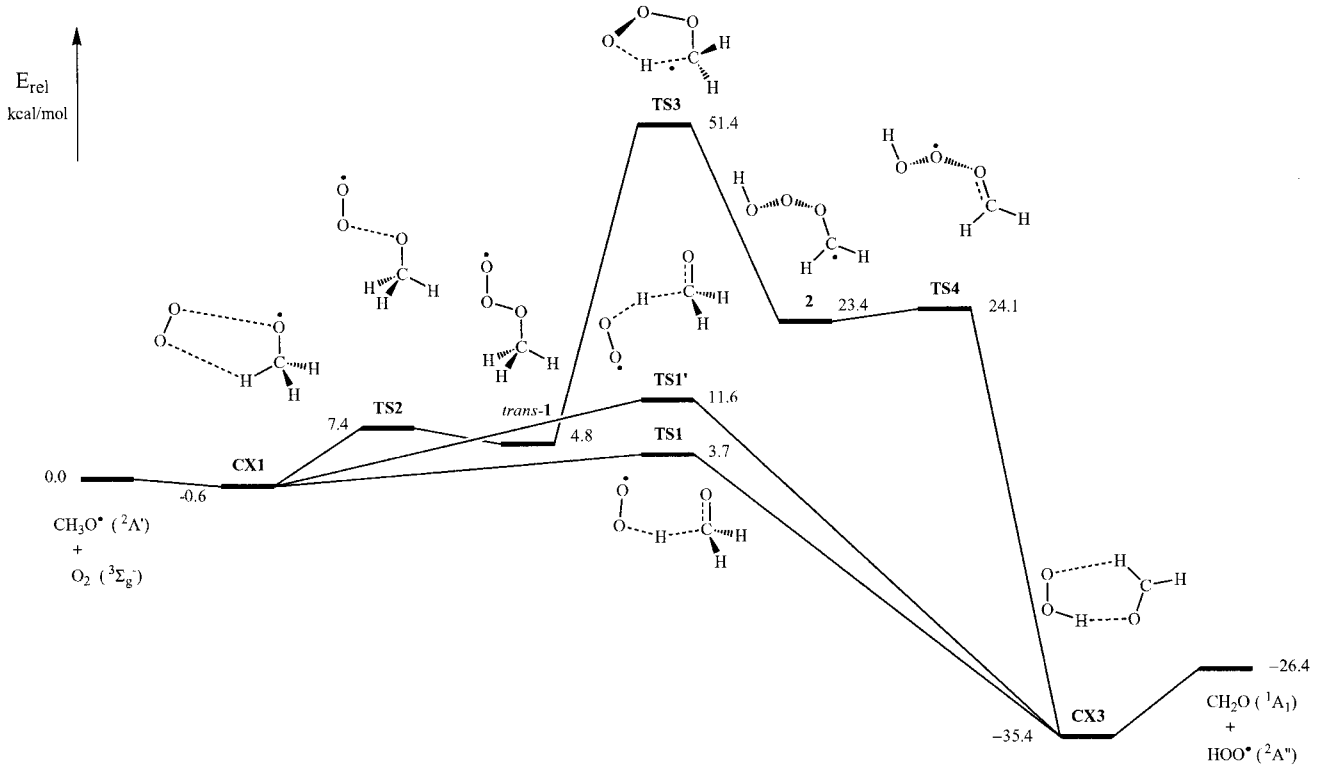

Figure 6. Schematic potential energy profiles showing the most relevant structures concerning the direct H atom transfer and stepwise pathways for the oxidation of $CH_3O^\bullet$ by O_2 forming $CH_2O + HO_2^\bullet$. Relative energy values were obtained from CCSD(T)/cc-pVTZ energy calculations at the CASSCF/6-311G(d,p) optimized geometries.

Table 1. Calculated Relative Energies (*E*, kcal/mol),[a] Zero-Point Vibrational Energies (ZPVE, kcal/mol),[b] Thermal Energy Corrections (TEC, kcal/mol),[b,c] and Absolute Entropies (*S*, eu)[b,c] for Various Species through the $CH_3O^\bullet + O_2$ Reaction

		E						
species	state	6-311G(d,p)	6-311+G(d,p)	6-311+G(3df,2p)	cc-pVTZ	ZPVE[d]	TEC	*S*
$CH_3O^\bullet + O_2$	$^2A''$	0.0	0.0	0.0	0.0	27.2 (0)	3.3	105.5
CX1	$^2A''$	−0.7	−0.8	−0.7	−0.6	27.4 (0)	4.6	97.2
TS1	$^2A''$	6.5	6.4	3.4	3.7 (3.8)	26.0 (1)	2.9	70.2
TS1′	$^2A''$	14.0	13.6	11.4	11.6 (11.7)	25.1 (1)	3.3	77.8
TS2	$^2A''$	8.6	8.2	7.2	7.4 (5.6)	28.7 (1)	3.2	74.0
trans-**1**	$^2A''$	10.0	9.6	5.3	4.8 (4.8)	30.3 (0)	3.1	72.5
TSGT	^2A	10.1	9.7	5.6	5.2	30.3 (1)	2.6	67.3
gauche-**1**	^2A	9.8	10.1	5.4	5.0	30.5 (0)	3.0	70.8
cis-**1**	$^2A''$	8.9	9.5	4.3	3.6 (3.7)	30.3 (1)	2.5	67.2
TS3	^2A	58.4	58.0	53.2	51.4	26.4 (1)	2.5	66.9
2	^2A	29.2	28.9	24.3	23.4	29.3 (0)	3.2	71.5
TS4	^2A	29.9	29.5	25.0	24.1	28.6 (1)	2.9	70.1
CX2	$^2A''$	−30.6	−31.0	−33.1	−32.7	28.4 (1)	3.9	83.1
CX3	$^2A'$	−33.5	−33.0	−35.4	−35.4	29.1 (0)	4.0	80.2
$H_2CO + HOO^\bullet$	$^2A''$	−23.9	−24.5	−26.5	−26.4 (−26.5)	27.1 (0)	3.6	106.9

[a] Calculated at the CCSD(T) level of theory with different basis sets using the CASSCF/6-311G(d,p) optimized geometries. The relative energies calculated at the RCCSD(T) level of theory are given in parentheses. [b] Obtained from CASSCF/6-311G(d,p) calculated harmonic vibrational frequencies. [c] At 298 K and 1 atm. [d] The number in parentheses is the number of imaginary frequencies.

trans/cis conformal change in **1**. In addition to **TSGT**, at the QCISD level of theory with both the 6-31G(d) and 6-311G(d,p) basis sets we located a torsional transition structure, **TSCG** (Supporting Information), connecting the *gauche*-**1** and *cis*-**1** local minima. Regarding the cis conformer of **1**, both the CASSCF and CISD calculations with the 6-31G(d) and 6-311G(d,p) basis sets predict its optimized structure, *cis*-**1** (Figure 3), to be the transition structure connecting the two equivalent structures (i.e., mirror images) of *gauche*-**1**. These findings are in clear contrast with the B3LYP/6-311G(d,p) and QCISD/6-311G(d,p) calculations of Jungkamp and Seinfeld[15,16] and our QCISD/6-31G(d) calculations, which predict *cis*-**1** to be a true local minimum on the PES.

At the CCSD(T)/cc-pVTZ + ZPVE level *cis*-**1** turns out to be the lowest energy conformer of radical **1**, lying 6.7 kcal/mol above the reactants, $CH_3O^\bullet + O_2$. This energy difference is significantly higher than the values of 0.87 and 2.01 kcal/mol predicted by the G2M(RCC) and CBS-APNO model chemistries.[16] On the other hand, the CCSD(T)/cc-pVTZ + ZPVE calculated energy difference of 1.2 kcal/mol between the cis and trans isomers of **1** is in close agreement with the values of 1.14 and 0.97 kcal/mol predicted by the latter two methods. At this point it is worth comparing the endoergicity of 8.3 kcal/mol, determined at the CCSD(T)/cc-pVTZ + ZPVE level, for the formation of gauche-**1** from $CH_3O^\bullet + O_2$ with the exoergicity of 30.5 kcal/mol reported by Schaefer and co-workers[66]

Table 2. Calculated Topological Properties of the Bond Critical Points and Net Atomic Charges in **TS1** and **TS1′** [a]

X−Y bond	r_X (Å)[b]	r_Y (Å)[c]	ρ_b (au)[d]	$\nabla^2\rho_b$ (au)[e]	ϵ[f]	Q_X	Q_Y
			TS1				
C2−H1	0.880	0.470	0.1383	−0.2088	0.0042	+0.852	+0.304
C2−O3	0.407	0.840	0.3694	0.3564	0.1179	+0.852	−0.972
O4−H1	0.887	0.342	0.1745	−0.1734	0.0474	−0.168	+0.304
O5−O3	1.227	1.186	0.0262	0.1030	0.1150	−0.016	−0.972
O4−O5	0.618	0.637	0.4777	−0.5707	0.0021	−0.168	−0.016
C2−H6	0.694	0.380	0.2888	−1.0700	0.0449	+0.852	−0.002
			TS1′				
C2−H1	0.853	0.457	0.1492	−0.2554	0.0152	+0.853	+0.286
C2−O3	0.408	0.844	0.3651	0.2869	0.0755	+0.853	−0.950
O4−H1	0.902	0.367	0.1565	−0.0787	0.0438	−0.141	+0.286
O4−O5	0.642	0.620	0.4676	−0.5354	0.0016	−0.141	−0.060
C2−H6	0.697	0.377	0.2895	−1.0750	0.0404	+0.853	+0.007

[a] Determined from Bader topological analysis of the CASSCF/6-311G(d,p) wave function. Atom numbering refers to Figure 2. [b] The distance between the bond critical point and the X atom. [c] The distance between the bond critical point and the Y atom. [d] Electronic charge density at the bond critical point. [e] Laplacian of ρ_b. [f] Bond ellipticity, defined as $\epsilon = (\lambda_1/\lambda_2) - 1$, where λ_1 and λ_2 are the negative eigenvalues of $\nabla^2\rho_b$ along the axes perpendicular to the bond path.

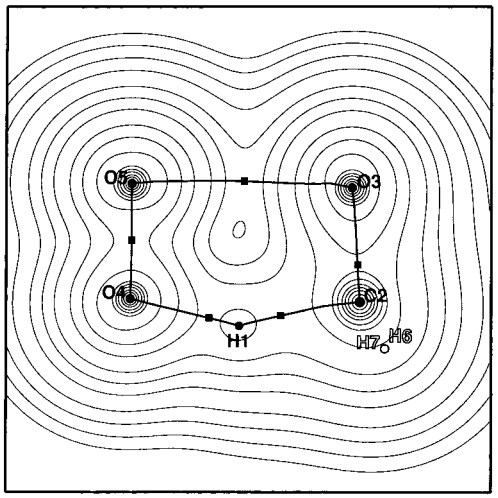

Figure 7. Contour plot in the C_s symmetry plane of the CASSCF/6-311G(d,p) electronic charge density of the transition structure **TS1** for direct H atom transfer from $CH_3O^\bullet$ to O_2. Bond critical points are denoted by squares. The labels of the nuclei that lie in the C_s plane are bold and those that do not lie in this plane are open.

for the formation of the gauche conformer of $CH_3CH_2OO^\bullet$ from $CH_3CH_2^\bullet + O_2$, calculated from ZPVE corrected CCSD(T)/DZP energies computed at CISD/DZP optimized geometries. This striking difference in the energy change accompanying the formation of the gauche conformer of the isoelectronic radicals $CH_3OOO^\bullet$ and $CH_3CH_2OO^\bullet$ is ascribed to the weak character of the central OO bond in the former radical, as compared with the expected greater strength of the CO bond in the latter radical.[67]

The second step of pathway (b) is the H atom transfer from C2 to O4 in the trioxy radical **1** forming the trioxomethyl radical intermediate **2**. As expected on the basis of the electronic considerations in Section II, this isomerization is found to take place via a puckered (C_1) ringlike transition structure **TS3**. In Figure 4, the CASSCF/6-311G(d,p) geometry of **TS3** is

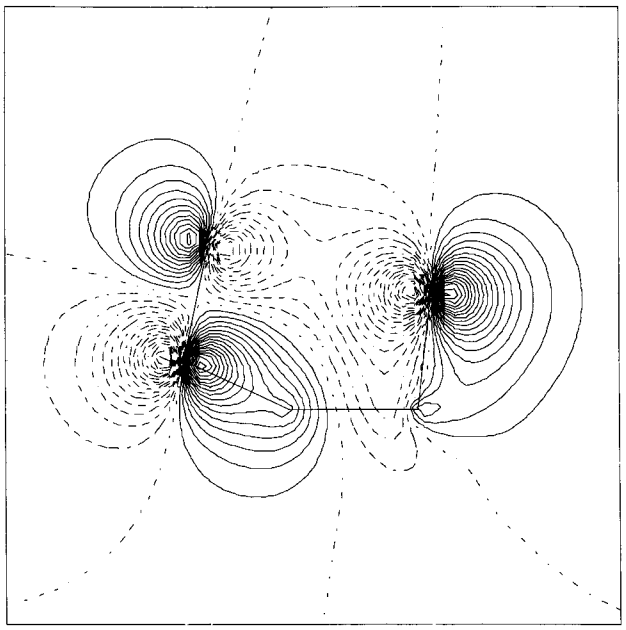

Figure 8. Contour plot in the C_s symmetry plane of the CASSCF/6-311G(d,p) molecular orbital associated with the forming π bond between the C2 and O3 atoms in transition structure **TS1** for direct H atom transfer from $CH_3O^\bullet$ to O_2.

compared with the geometry optimized at the CISD/6-311G-(d,p) level, rather than that with the QCISD/6-311G(d,p) geometry. The geometry optimization at the latter level of theory was not fully accomplished because the iterative procedure involved in the resolution of the QCISD equations did not converge in the last steps of the optimization. It is important to note that we have not found any transition structure for the intramolecular H-transfer **1** → **2** employing the B3LYP method with the 6-311G(d,p) basis set. We tried to locate one using as the initial geometry that of **TS3** optimized either at the CASSCF or CISD level with the 6-311G(d,p) basis set. However, along the geometry optimization the O5O3 bond was continuously elongated and the computation did not result in any saddle point. On the other hand, it is remarkable that the geometry of **TS3** is qualitatively similar to the ringlike transition structure of C_1 symmetry located at the CISD/DZP level of theory for the related H atom shift in $CH_3CH_2OO^\bullet$ leading to $^\bullet CH_2CH_2OOH$.[66]

At the CCSD(T)/cc-pVTZ level, a potential energy barrier of 46.4 kcal/mol is predicted for the *gauche*-**1** → **2** isomerization through **TS3**. The main reason of this high barrier is the formation of a highly strained five-membered ring in going from **1** to transition structure **TS3**. In fact, the inherent tendency of the oxygen chain to assume a skew geometry in the hydrogen polyoxides (HO_nH) to diminish lone pair repulsion between the O atoms is well-known.[68] Thus in H_2O_3 the free valences of the terminal O atoms point to directions perpendicular to the OOO plane, the OH bonds being on opposite sides of the plane.[69] Analogously, the O4H1 and O3C2 bonds in **2** are nearly perpendicular to the O4O5O3 plane, while in **TS3** these bonds are far from being perpendicular to this plane, as indicated by the H1O4O5O3 and C2O3O5O4 dihedral angles of 37.9 and 49.6°, respectively. Furthermore, we note that in **TS3** the C2H1O4 angle is 30.9° smaller than in the strain-free transition structure **TS1′** calculated for the intermolecular H-transfer between $CH_3O^\bullet$ and O_2.

(66) Quelch, G. E.; Gallo, M.; Shen, M.; Xie, Y.; Schaefer, H. F., III; Moncrieff, D. *J. Am. Chem. Soc.* **1994**, *116*, 4953.

(67) The experimental average bond energies of the O−O and C−O single bonds are 33.2 and 84.0 kcal/mol, respectively (Cumper, C. W. N. *Wave Mechanics for Chemists;* Heinemann: London, 1966; p 219).

(68) For a review, see: Mckay, D. J.; Wright, J. S. *J. Am. Chem. Soc.* **1998**, *120*, 1003.

(69) Cremer, D. *J. Chem. Phys.* **1978**, *69*, 4456.

The optimized geometry of the trioxomethyl radical intermediate **2**, which is formed after **TS3** is cleared, is shown in Figure 4. At the CCSD(T)/cc-pVTZ level, this structure lies 23.4 kcal/mol above the energy of $CH_3O^\bullet + O_2$ and is 18.4 kcal/mol less energetic than *gauche*-**1**. After including the ZPVE corrections, this energy separation is found to be 17.2 kcal/mol. This value is comparable to the energy difference of 20.2 kcal/mol between the radical intermediates *gauche* CH_3CH_2-$OO^\bullet$ and $^\bullet CH_2CH_2OOH$ obtained by Schaefer and co-workers[66] from ZPVE corrected CCSD(T)/DZP energies calculated at CISD/DZP optimized geometries. We have not found any equilibrium structure for the trioxomethyl radical **2** employing the B3LYP method with the 6-311G(d,p) basis set. We tried to locate one using as initial geometry that of **2** optimized either at the CASSCF or QCISD level of theory with the 6-311G(d,p) basis set. However, along the geometry optimization the O5O3 bond undergoes a continuous elongation leading to the **CX3** complex. In contrast, CISD calculations with the 6-311G(d,p) basis set yielded for radical **2** an optimized equilibrium geometry close to those obtained at the CASSCF and QCISD levels of theory.

The last step of pathway (b) is the easy homolytic cleavage of the weak central OO bond in **2**, leading to the hydrogen-bonded $[CH_2O\cdots HOO^\bullet]$ complex, **CX3**. This process is highly exoergic (−59.0 kcal/mol at the CCSD(T)/cc-pVTZ + ZPVE level of computation) and takes place via the transition structure **TS4** (Figure 5) with a potential energy barrier of only 0.7 kcal/mol. It appears, therefore, that the intermediate **2** is a shallow minimum on the PES. In accordance with the high exoergicity and low barrier predicted for the process **2** → **CX3**, **TS4** possesses an early characteristic, as shown by the small differences found between the geometries optimized for **2** and **TS4**. Actually, the transition vector associated with the imaginary frequency of **TS4** corresponded chiefly to the rotation of the methylene group about the C2O3 bond combined with a small lengthening of the O5O3 bond.

In addition to pathway (b), we investigated the concerted $HO_2^\bullet$ elimination in the trioxy radical intermediate **1**, namely the second step (eq 5) of the addition/elimination pathway (c). We tried to locate a transition structure connecting **1** with $CH_2O + HO_2^\bullet$ at the CASSCF and QCISD levels of theory with the 6-311G(d,p) basis. Starting the transition structure search at the B3LYP/6-311G(d,p) optimized geometry of **TSB** reported by Jungkamp and Seinfeld,[16] the optimization led in each case to the transition structure for direct H atom transfer from $CH_3O^\bullet$ to O_2 (i.e., **TS1**). This unexpected result prompted us to perform an IRC calculation starting at the B3LYP/6-311G(d,p) optimized structure of **TSB** with the aim of comparing it with the IRC profile shown in Figure 3 of ref 16 proving the connection of *cis*-**1** and $CH_2O + HO_2^\bullet$ via **TSB**. Our IRC[70] calculation revealed that **TSB** is connected to the hydrogen-bonded complex **CX2** in the forward direction and to the loosely bound complex **CX1** in the reverse direction. For the sake of completeness, the values of the most relevant geometrical parameters of the structures optimized at the B3LYP/6-311G(d,p) level for the **CX1**, **CX2**, and **CX3** complexes are given in Figure 2. The discrepancy between the two IRC calculations being compared is ascribed to the different quality of the basis sets employed in each case. In fact, our IRC calculation was carried out with the 6-311G(d,p) basis set, while the IRC profile shown in ref 16 was obtained by using the 3-21G(d,p) basis,[71] which is far too low to be reliable. At any rate, the results of our IRC calculations at the CASSCF/6-31G(d), CASSCF/6-311G(d,p), QCISD/6-31G(d), QCISD/6-31G(d,p), B3LYP/6-31G(d,p), and B3LYP/6-311G(d,p) levels of theory prove that **TS1** corresponds to the transition structure for direct H atom transfer from $CH_3O^\bullet$ to O_2. Further attempts to locate at either the CASSCF or QCISD levels of theory a transition structure for the concerted $HO_2^\bullet$ elimination in *cis*-**1**, leading either to a loosely bound $[CH_2O^\bullet\cdot\cdot HO_2^\bullet]$ complex or $CH_2O + HO_2^\bullet$, were unsuccessful.

In summary, the stepwise pathway (b) $CH_3O^\bullet + O_2 \rightarrow$ **CX1** → **TS2** → *trans*-**1** → **TSGT** → *gauche*-**1** → **TS3** → **2** → **TS4** → **CX3** → $CH_2O + HO_2^\bullet$ has as the rate determining step the formation of the radical intermediate **2** with a global potential energy barrier of 51.4 kcal/mol. This mechanism cannot compete with the direct H atom tranfer pathway (a) $CH_3O^\bullet + O_2 \rightarrow$ **CX1** → **TS1** → **CX3** → $CH_2O + HO_2^\bullet$ involving a potential energy barrier of only 3.7 kcal/mol.

C. Arrhenius Parameters. Assuming that the oxidation of $CH_3O^\bullet$ by O_2 takes place through pathway (a) and **TS1** is the transition state, an activation energy (E_a) of 2.8 kcal/mol and a preexponential factor (A) of 3.5733×10^{-14} molecule cm^3 s^{-1} at 298 K are predicted from the relative energies computed at the RCCSD(T)/cc-pVTZ level and the CASSCF/6-311G(d,p) calculated harmonic vibrational frequencies. These Arrhenius parameters give a classical rate constant of 2.9×10^{-16} molecule^{-1} cm^3 s^{-1} at 298 K. The recommended experimental[9] parameters are $E_a = 1.788 \pm 0.596$ kcal/mol and $A = 3.9 \times 10^{-14}$ cm^3 molecule^{-1} s^{-1} and the experimental rate constant is 1.9×10^{-15} molecule^{-1} cm^3 s^{-1} at 298 K. Thus the calculated classical rate constant is about 1 order of magnitude lower than the experimental rate constant. By using eq 10 a quantum mechanical tunneling correction factor $\Gamma^* = 9.073$ was computed at 298 K, which leads to a predicted rate constant of 2.7×10^{-15} molecule^{-1} cm^3 s^{-1} in good agreement with the experimental value. This provides further support to the direct H atom transfer mechanism for the oxidation of $CH_3O^\bullet$ by O_2.

V. Summary and Conclusions

The most relevant energetic results of the present study are summarized in Figure 6. In contrast to a recent theoretical study predicting an addition/elimination mechanism forming the methyltrioxy radical $CH_3OOO^\bullet$ as intermediate, the oxidation of $CH_3O^\bullet$ by O_2 leading to $CH_2O + HO_2^\bullet$ occurs through a direct H atom transfer pathway involving the ringlike transition structure **TS1** with a potential energy barrier of 3.7 kcal/mol. **TS1** shows an intermolecular noncovalent O···O bonding interaction, which lowers its potential energy with respect to that of the noncyclic transition structure **TS1′** by about 8 kcal/mol. This noncovalent interaction arises from the polarization of both oxygen atoms caused by the forces exerted on their nuclei by the electronic charge accumulated on the oxygen atom of the CH_3O moiety due to the forming CO π bond. The 1,4-hydrogen shift in $CH_3OOO^\bullet$ is not accompanied by $HO_2^\bullet$ elimination but leads to the trioxomethyl radical $^\bullet CH_2OOOH$ via a puckered ringlike transition structure, lying 50.6 kcal/mol above the energy of the reactants. The good agreement between

(70) Calculated at the B3LYP/6-311G(d,p) level in mass-weighted internal coordinates, using the second-order algorithm of Gonzalez and Schlegel (ref 41) implemented into GAUSSIAN 94, with a step size of 0.05 bohr·amu$^{1/2}$.

(71) In ref 16 it is stated that the IRC profile was calculated at the B3LYP/6-31G(d,p) level. Although the energy calculated at this level of theory for **TSB** was not reported, a value close to −263.917 hartrees can be estimated from Figure 3 in ref 16. This value is by far much higher than the energy of −265.36587 hartrees we have computed at the B3LYP/6-31G(d,p) level for **TSB**. An anonymous reviewer has indicated that a number around −263.917 hartrees arises from calculations at the B3LYP/3-21G(d,p) level and concluded that the figure presenting the IRC profile in ref 16 is most probably labeled wrong.

the calculated (2.7×10^{-15} molecule^{-1} cm^3 s^{-1}) and experimental (1.9×10^{-15} molecule^{-1} cm^3 s^{-1}) values of the rate constant at 298 K for reaction 1 gives strong support to the direct H atom transfer mechanism for the oxidation of $CH_3O^{\bullet}$ by O_2 in the gas phase.

Acknowledgment. This research was supported by the DGICYT (Grants PB95-0278-C01 and PB95-0278-C02). Calculations described in this work were performed on a HP9000 J280/2 workstation at the University of Barcelona, an IBM RS6000 workstation at the CID of CSIC, and the IBM SP2 at the Centre de Supercomputació de Catalunya. The authors also wish to thank Professor Sigrid D. Peyerimhoff and Dr. Michael W. Schmidt for providing a copy of MRD-CI and GAMESS codes, respectively. We also express appreciation to Professor Richard F. W. Bader for the PROAIM and EXTREME programs and to Dr. P. L. A. Popelier for the MORPHY97 program.

Supporting Information Available: Tables S1−S6 summarizing total energies, zero-point vibrational energies, absolute entropies, topological properties of bond critical points, and net atomic charges, calculated at different levels of theory, of all structures reported in this paper and a figure showing the optimized geometries of O_2, $CH_3O^{\bullet}$, $HO_2^{\bullet}$, and CH_2O (PDF). This material is available free of charge via the Internet at http://pubs.acs.org.

JA981926Y